**Electronic supplementary information for**

# In situ electrochemical synthesis of Pd aerogels as highly efficient anodic electrocatalysts for alkaline fuel cells

Chen Wang[+,a], Wei Gao[+,a], Xinhao Wan[+,a], Bin Yao[a], Wenjing Mu[a], Jie Gao[b,*], Qiangang Fu[a,*], Dan Wen[a,*]

[a] *State Key Laboratory of Solidification Processing, School of Materials Science and Engineering, Northwestern Polytechnical University, Xi'an, 710072, P. R. China*

[b] *School of Life Sciences, Northwestern Polytechnical University, Xi'an, 710072, P. R. China*

[+] C. Wang, W. Gao, and X. Wan contributed equally to this work.

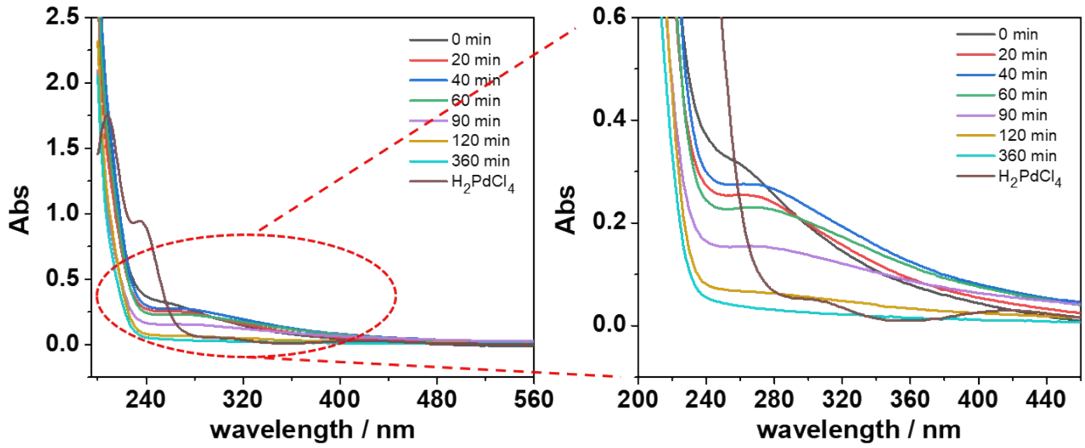


Figure S1. UV-vis spectra for $H_2PdCl_4$ and the supernatants of samples with different reacting times.

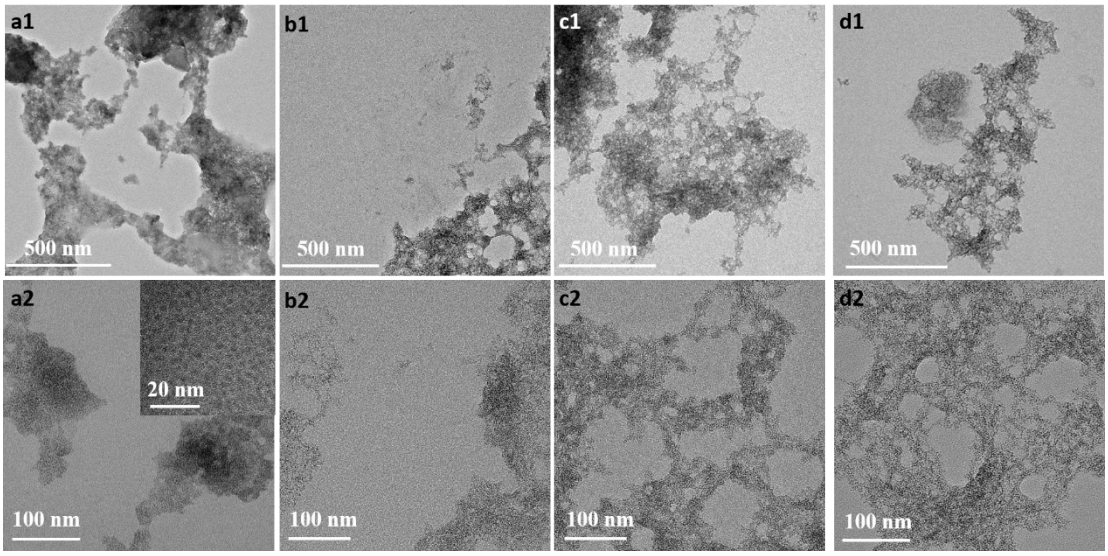


Figure S2. TEM images of $PdO_x$ samples with different reacting times: (a) 0 minute, (b) 20 minutes, (c) 40 minutes, and (d) 120 minutes.

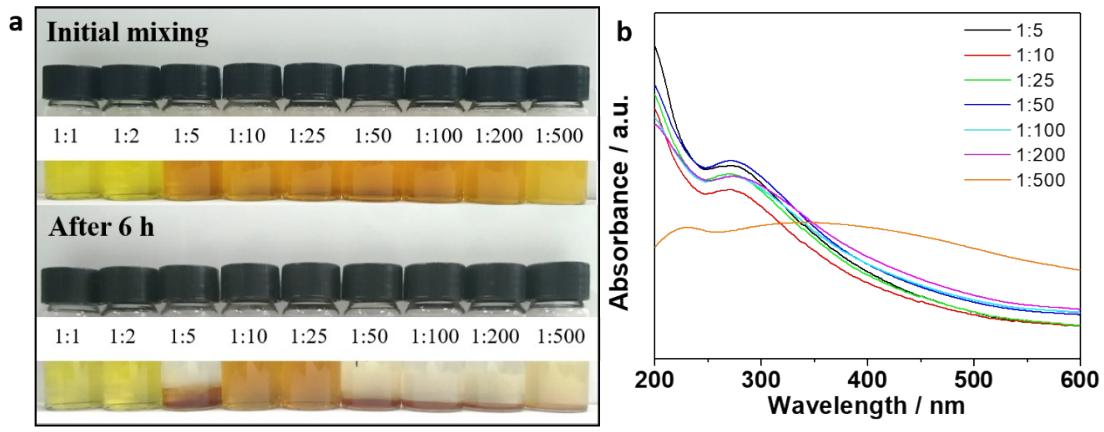


Figure S3. (a) Optical images of $H_2PdCl_4$ and $Na_2CO_3$ mixture solutions with different molar ratios of 1:1, 1:2, 1:5, 1:10, 1:25, 1:50, 1:100, 1:200, and 1:500 before and after 6 hours' reaction. (b) UV-vis spectra of sediments for the samples with $H_2PdCl_4$ to $Na_2CO_3$ molar ratios of 1:5, 1:10, 1:25, 1:50, 1:100, 1:200, and 1:500 after 6 hours' reaction.

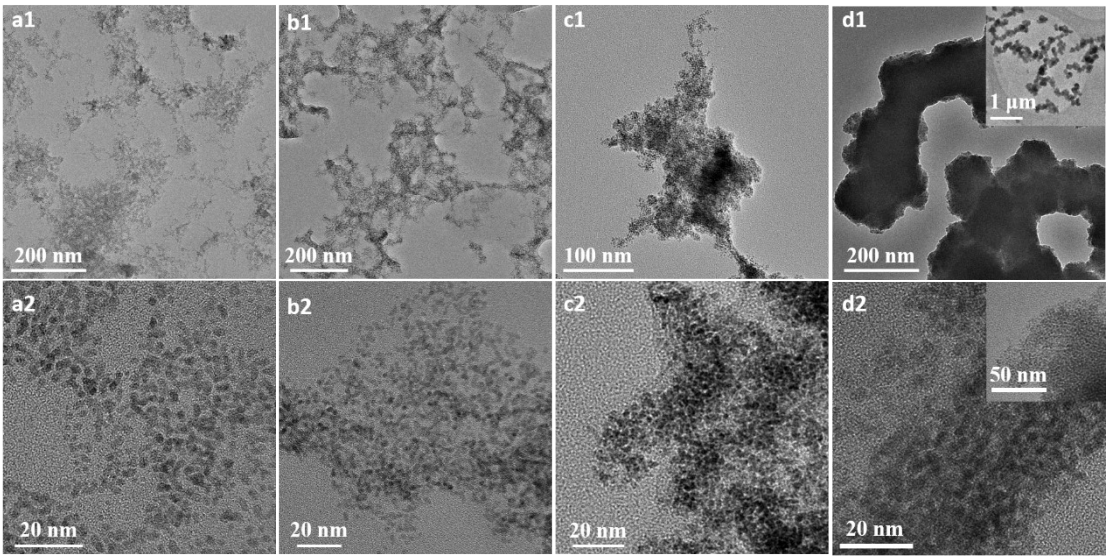


Figure S4. Typical TEM images for $PdO_x$ hydrogels with different $H_2PdCl_4$ to $Na_2CO_3$ molar ratios after 6 hours' reaction: (a) 1:5, (b) 1:100, (c) 1: 200, and (d) 1:500.

**Effect of $H_2PdCl_4$ to $Na_2CO_3$ molar ratio**

Firstly, the molar ratios of $H_2PdCl_4$ to $Na_2CO_3$ ranged from 1:1 to 1:500 with a fixed amount of $H_2PdCl_4$ and solution volume were performed. As optical images shown in Figure S3a, clear solutions were obtained after the initial mixing of different ratios of $H_2PdCl_4$ and $Na_2CO_3$. After 6 hours, $PdO_x$ nanoparticles were obtained for samples with $H_2PdCl_4$ to $Na_2CO_3$ ratios larger than 1:5, as confirmed by the UV-vis spectra from their corresponding solid sediments (Figure S3b). TEM images (Figure S4) of above samples revealed that the ratio of 1:100 was better for the formation of $PdO_x$ hydrogels with uniform nanoparticle assembling. Besides, a lower ratio of 1:5 led to the loosely connected framework structures by nanoparticles, while higher ratios of 1:200 and 1:500 resulted in the serious aggregation of nanoparticles, all of which are not favored for building aerogel structure.

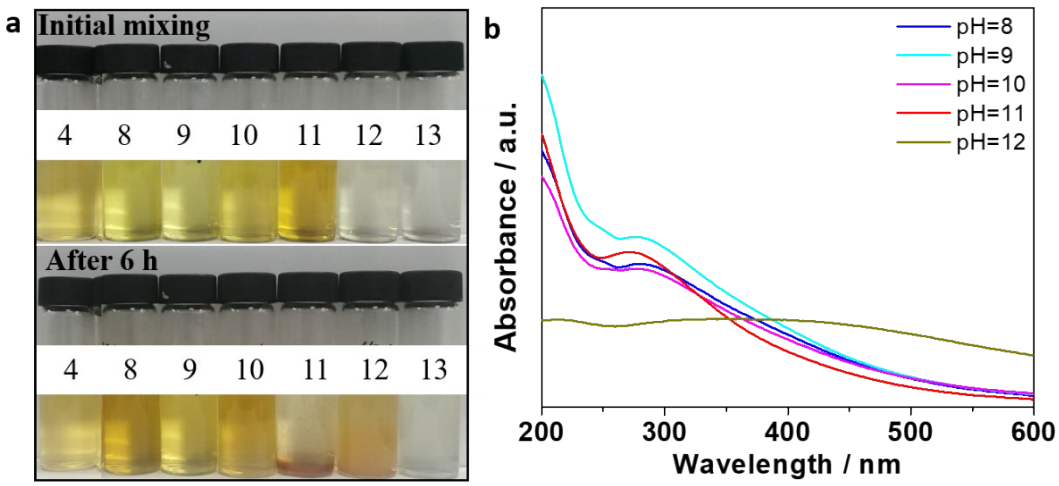


Figure S5. (a) Optical images of $H_2PdCl_4$ and $Na_2CO_3$ mixture solutions with different pH values of 4, 8, 9, 10, 11, 12, and 13 before and after 6 hours' reaction. (b) UV-vis spectra of sediments for the samples with pH values of 8, 9, 10, 11, and 12 after 6 hours' reaction.

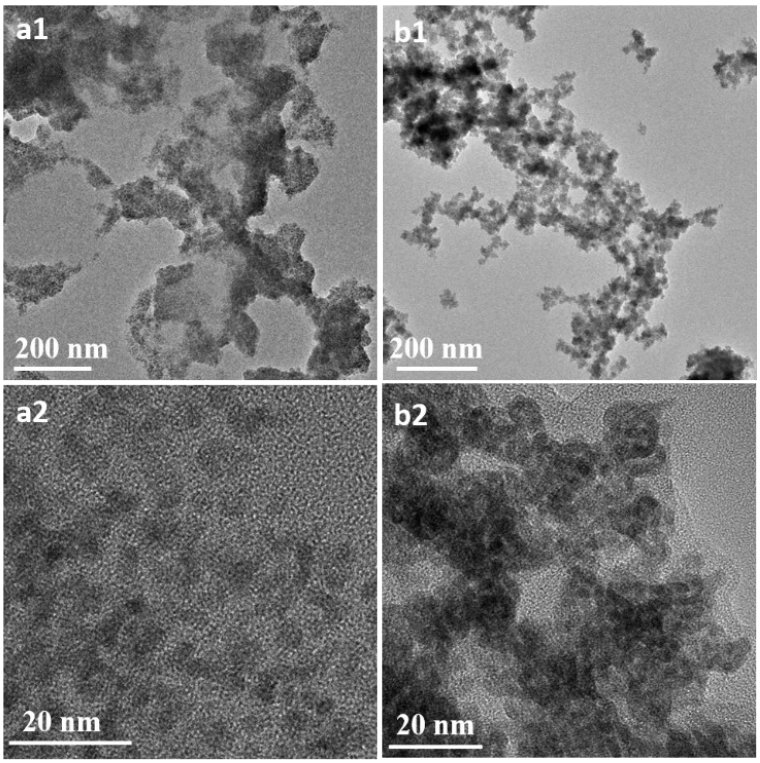


Figure S6. Typical TEM images for $PdO_x$ hydrogels with different pH values after 6 hours' reaction: (a) pH=8, and (b) pH=12.

**Effect of pH in solution**

The effect of pH value was discussed by regulating the pH values from 4 to 13 with a fixed molar ratio (1:100) of $H_2PdCl_4$ to $Na_2CO_3$. Optical images after 6 hours' reaction in **Figure S5a** indicated the formation of $PdO_x$ nanoparticles under the pH from 8 to 12, as also checked by UV-vis spectra (**Figure S5b**). However, apparent gels were only observed for the sample with the pH value of 11. As TEM images exhibited in **Figure S6**, the pH value of 8 would lead to the sediments of $PdO_x$ nanoparticles without clear pore structures, while the pH value of 12 caused the assembling of nanoparticles into larger building blocks to form aerogels. From this point, a weak basic condition of pH=11 is preferred for the $PdO_x$ gelation process.

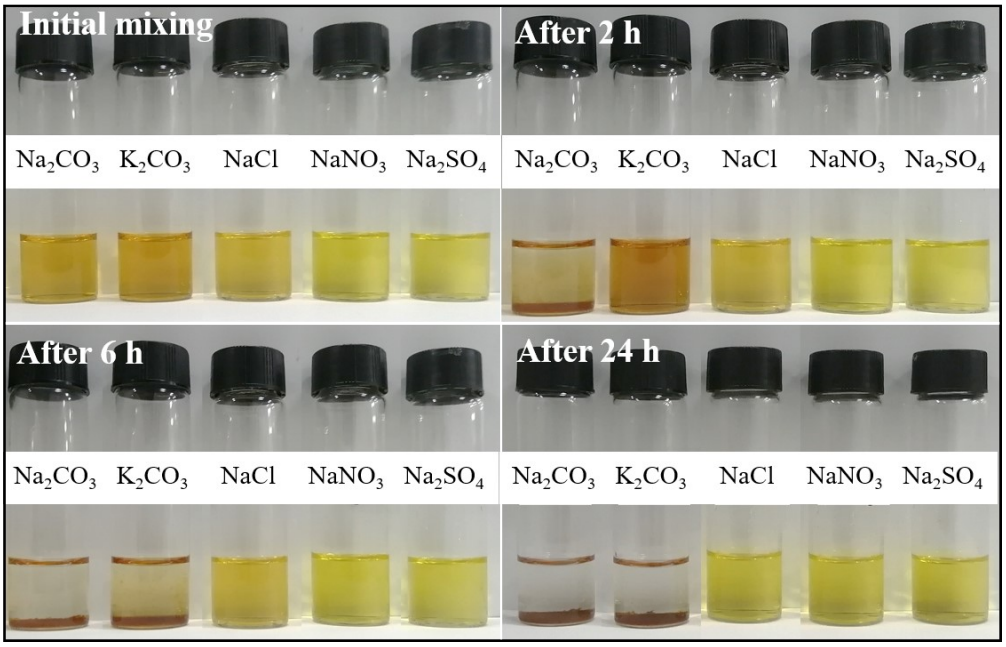


Figure S7. Optical images for the mixture solution of $H_2PdCl_4$ with $Na_2CO_3$, $K_2CO_3$, NaCl, $NaNO_3$, and $Na_2SO_4$ under different reacting times.

**Effect of metal salts**

Lastly, different metal salts of $Na_2CO_3$, $K_2CO_3$, NaCl, $NaNO_3$, and $Na_2SO_4$ with the same molar ratio are employed to research the universality of this hydrolysis method. The optical images (**Figure S7**) demonstrated that no sediments were formed with the salts of NaCl, $NaNO_3$, and $Na_2SO_4$ after 24 hours. The gelation of $PdO_x$ hydrogels could be realized for both $Na_2CO_3$ and $K_2CO_3$, while a longer time of 24 hours was required with $K_2CO_3$ as the reactant. Thus, $Na_2CO_3$ is favored for the faster gelation of $PdO_x$ aerogels under the optimized synthetic condition due to its hydrolysis to provide a weak basic condition, and high salt concentration to salt out hydrogel.

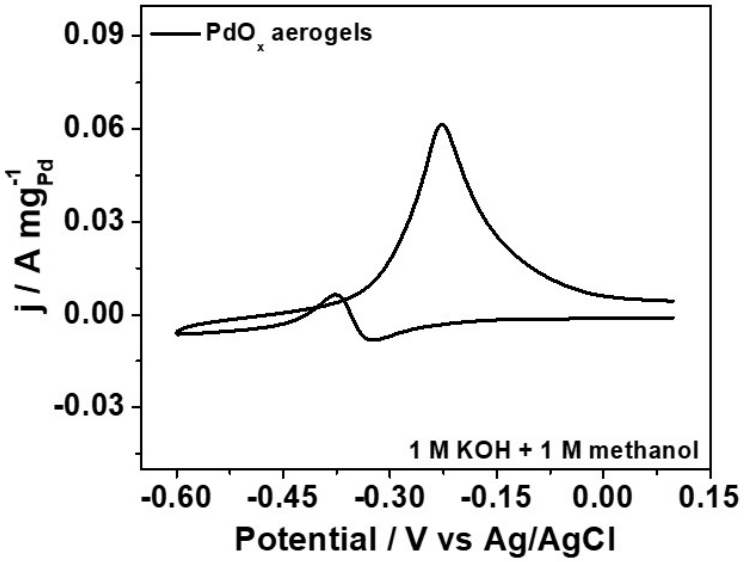


Figure S8. CV curve for $PdO_x$ aerogels on GC electrode (with Pd mass of 1 ug) in the 1 M KOH solution containing 1 M methanol with a scan rate of 50 mV/s.

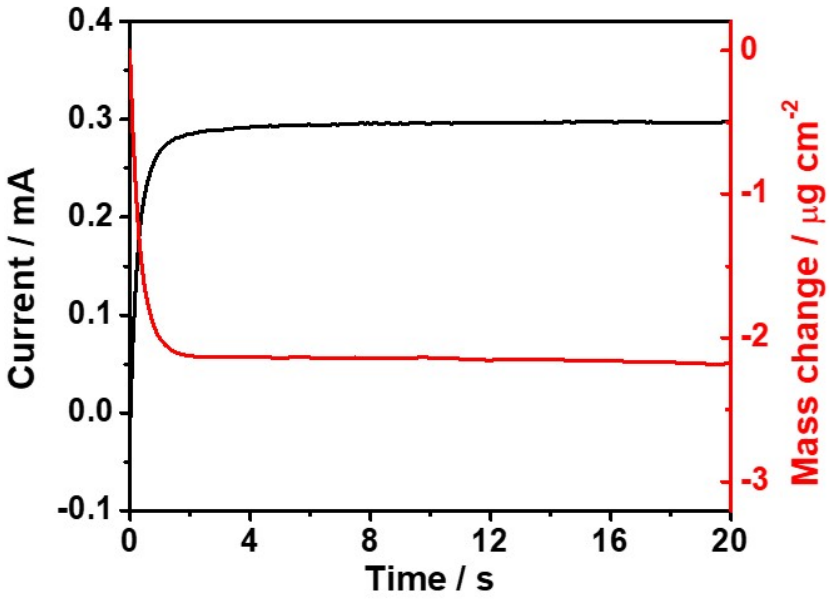


Figure S9. The EQCM signals and corresponding mass changes for $PdO_x$ aerogels during the in situ electrochemical activation.

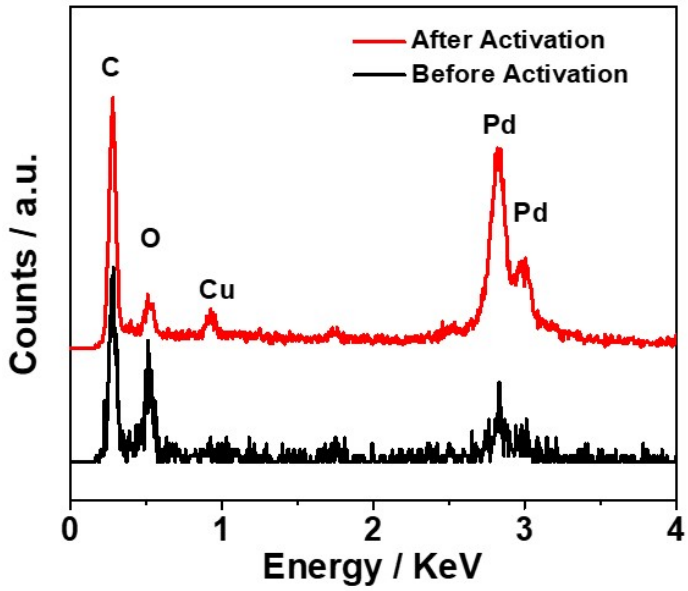


Figure S10. TEM-EDS spectra for $PdO_x$ aerogels before and after *in situ* electrochemical reduction.

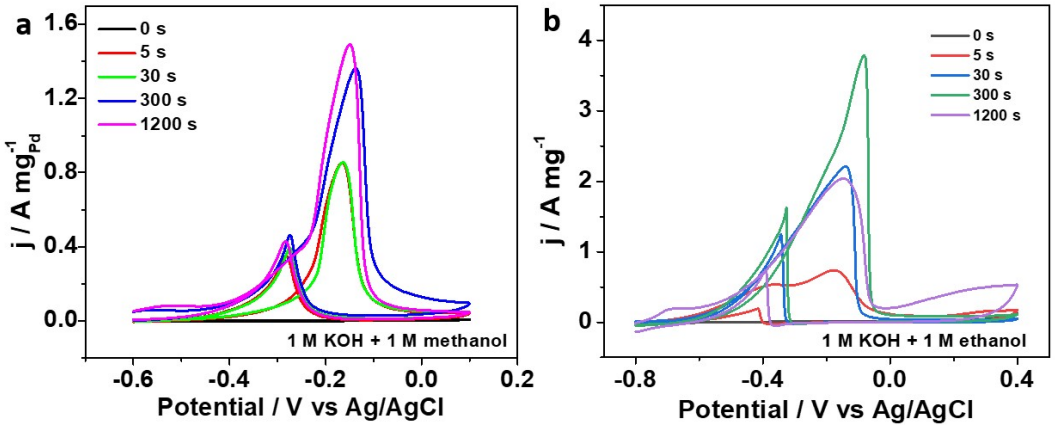


Figure S11. CV curve for Pd aerogels from the reduction of $PdO_x$ aerogels with different reducing times on Ti plate (with Pd mass of 6 ug) in the 1 M KOH solution containing (a) 1 M methanol, and (b) 1 M ethanol with the scan rate of 50 mV/s.

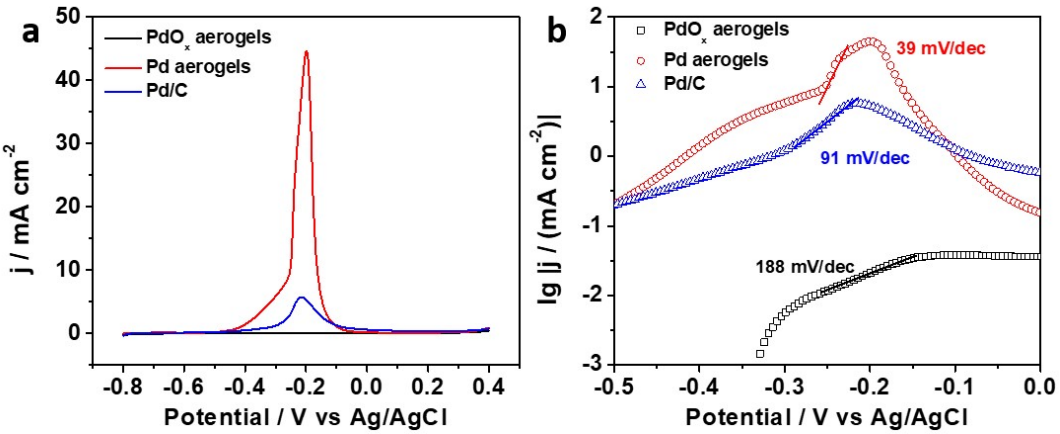


Figure S12. (a) LSV curves for $PdO_x$, Pd aerogels and Pd/C in 1 M KOH solution containing 1 M ethanol with the scan rate of 5 mV/s. (b) Tafel slopes derived from LSV curves in (a).

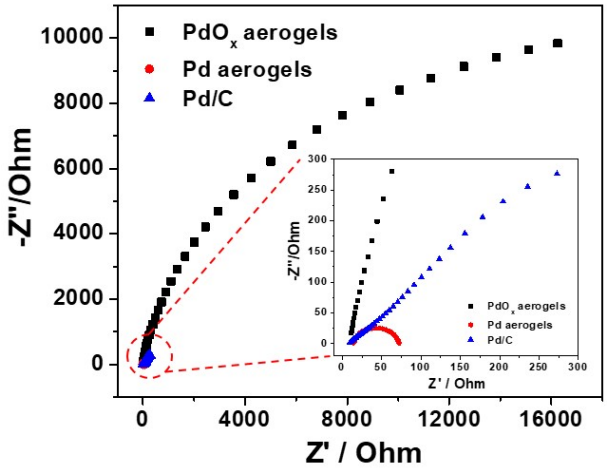


Figure S13. The Nyquist plots for Pd/C, Pd, and $PdO_x$ aerogels in 1 M KOH solution containing 1 M methanol.

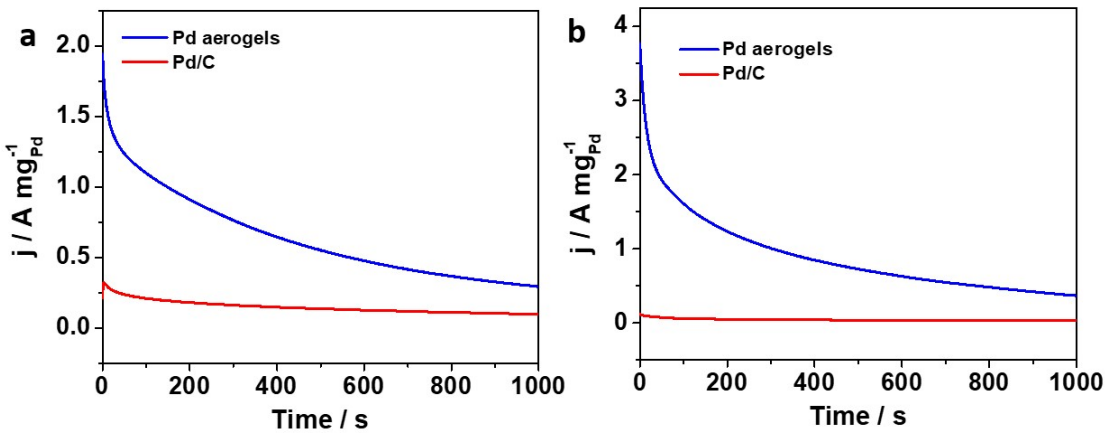


Figure S14. Durability tests for Pd aerogels in (a) 1 M KOH solution containing 1 M methanol, and (b) 1 M KOH solution containing 1 M ethanol.

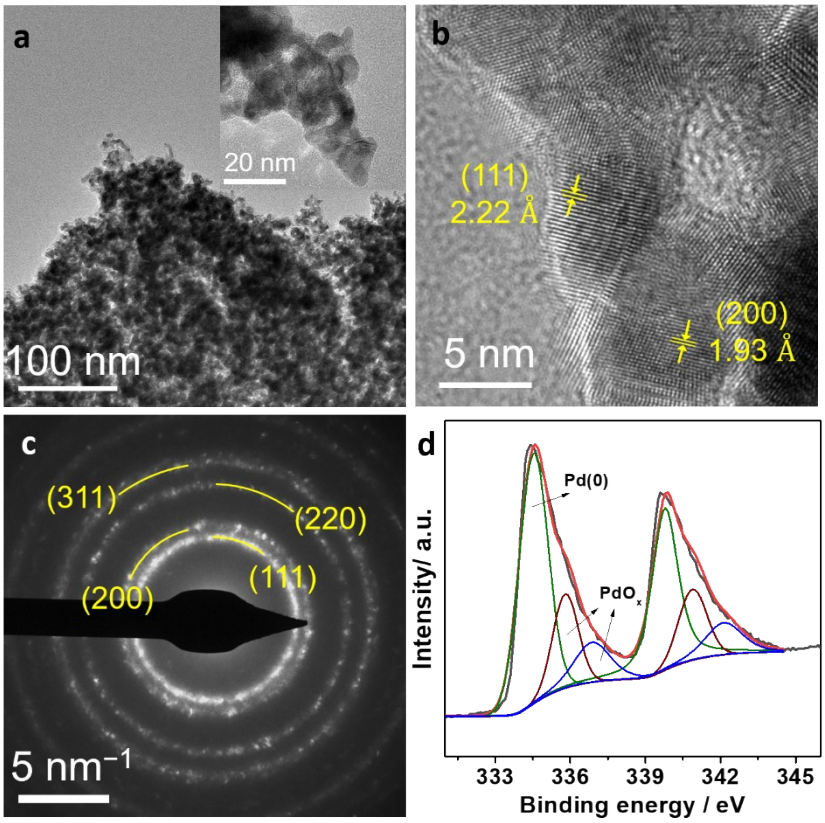


Figure S15. (a) TEM images, (b) HRTEM image, (c) SAED pattern for the used Pd aerogels. (d) Pd 3d orbital for the used Pd aerogels.

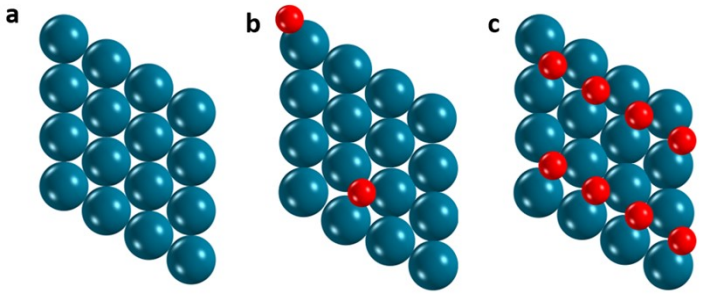


Figure S16. Surface composites for (a) pure Pd, (b) Pd aerogels, and (c) $PdO_x$ aerogels based on 4×4 Pd (111) plane. The balls with white, black, red, and blue represent H, C, O, and Pd atoms, respectively.

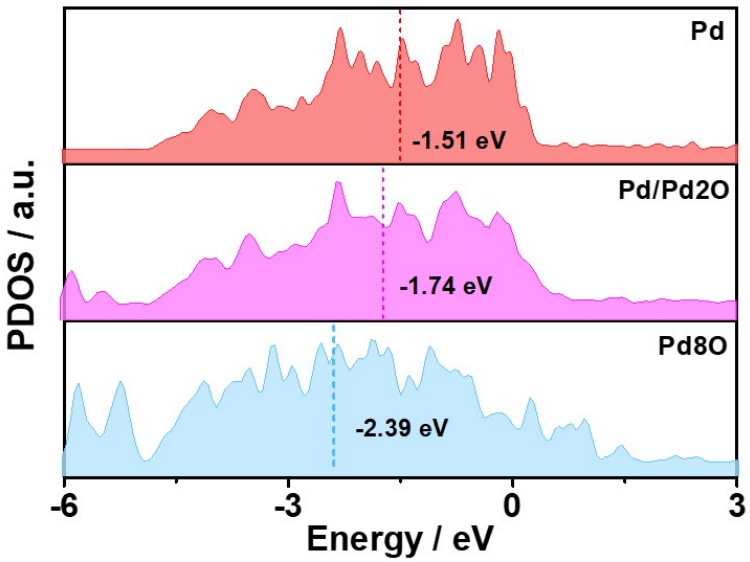


Figure S17. PDOS curves of Pd d orbital for metal Pd, Pd aerogels and $PdO_x$ aerogels.

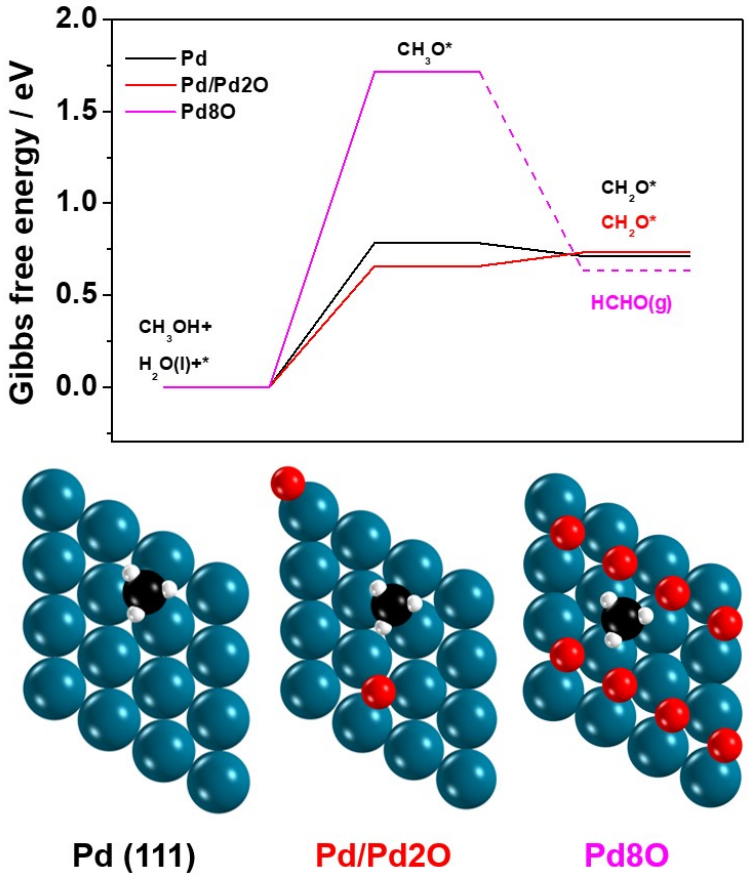


Figure S18. The Gibbs free energy diagram for absorbing *$CH_3O$ intermediate on different samples. The balls with white, black, red, and blue represent H, C, O, and Pd atoms, respectively.

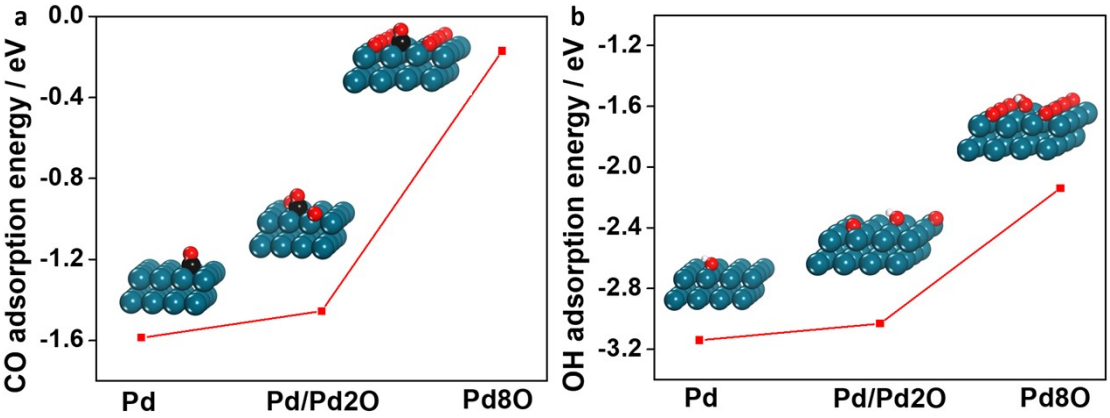


Figure S19. The *CO and *OH adsorption energy on the site of different samples.

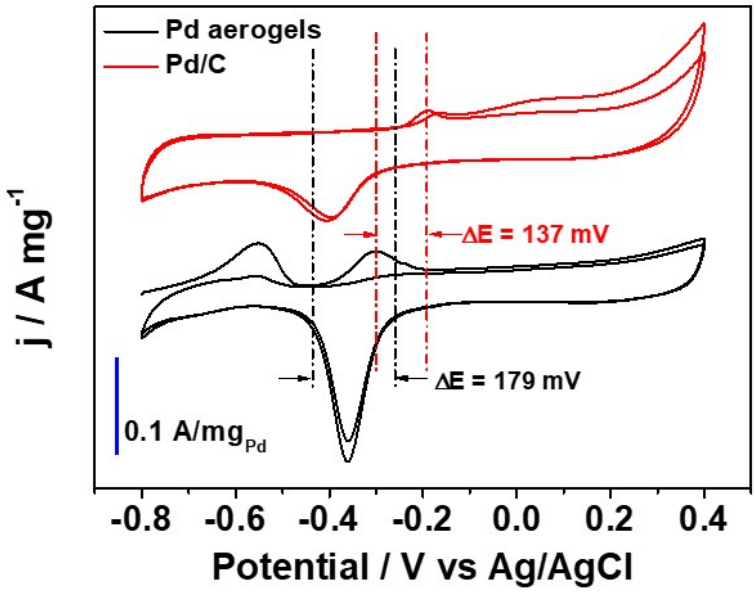


Figure S20. Preabsorbed CO stripping CV curves for Pd aerogels and Pd/C in 1 M KOH solution with a scan rate of 50 mV/s.

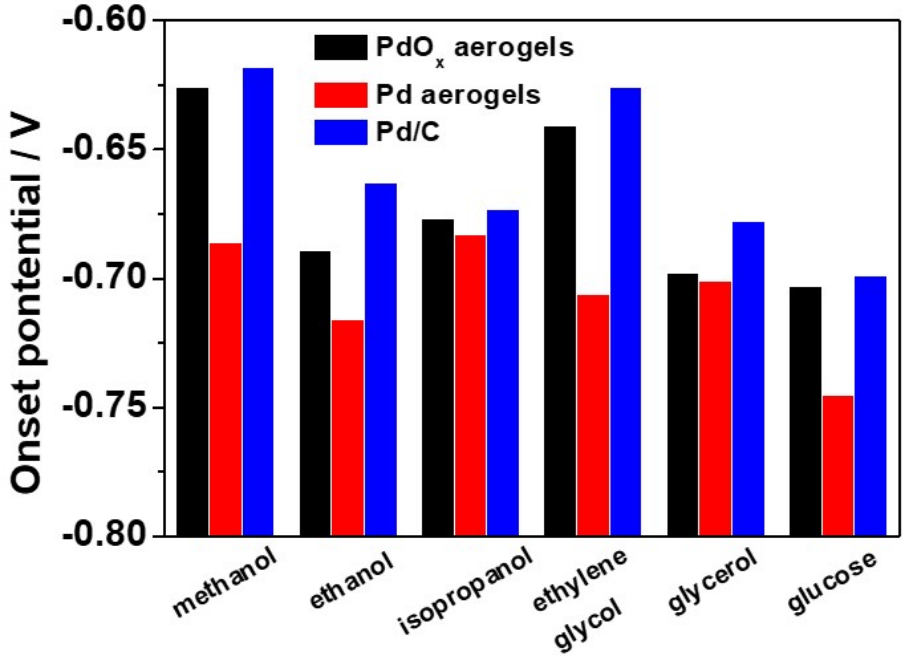


Figure S21. Comparison of onset potentials for various fuels with $PdO_x$, Pd aerogels and Pd/C as the anodic electrocatalysts.

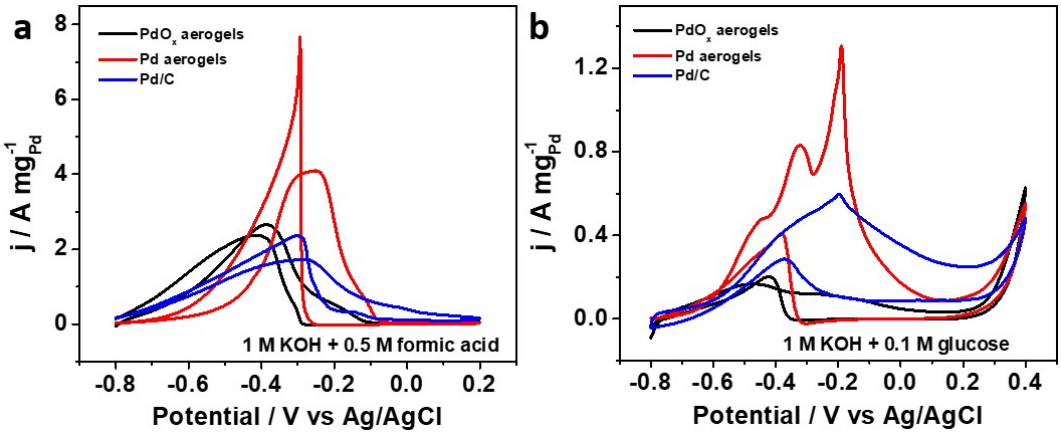


Figure S22. Electrochemical performances for commercial Pd/C, $PdO_x$ aerogels and Pd aerogels with different chemicals as fuels. (a) CV curves in 1 M KOH solution containing 0.5 M formic acid with a scan rate of 50 mV/s. (b) CV curves in 1 M KOH solution containing 0.1 M glucose with a scan rate of 50 mV/s.

For the glucose oxidation reaction, the peak at about -0.3 V is ascribed to the oxidation of Pd to Pd oxide in the mixture KOH and glucose solution both Pd aerogels and Pd/C, suggesting the partial oxidation of Pd in the forward scanning. Moreover, the similar peak was also observed in Figure 2b at the potential of about -0.3 V for the electrochemical behavior of Pd aerogels, which is the typical oxidation signal for metallic Pd.

Table S1. Comparison in specific surface areas for different noble metal aerogels.

| Sample | Specific surface area/ $m^2 g^{-1}$ | Reference |
|---|---|---|
| $PdO_x$ aerogels | 177.7 | this work |
| Au aerogels | 37 | [1] |
| Pd aerogels | 108 | [2] |
| PVP-Au aerogels | 42.6 | [3] |
| Au-Pd aerogels | 83.6 | [4] |
| Au-Pt aerogels | 74.5 | [4] |
| Pt nanocubes aerogels | 35 | [5] |
| Pd aerogels | 122.7 | [6] |
| Au aerogels | 59.8 | [7] |
| $Pd_3Cu_1$ aerogels | 99.8 | [8] |
| Au-Pd aerogels | 47.7 | [9] |
| $Pd_{10}Au$ aerogels | 105 | [9] |
| Ni-$Pd_{80}Pt_{20}$ | 95.4 | [10] |
| L-Pd aerogels | 48 | [11] |
| $Ru_{0.7}Co_{0.3}$ aerogel | 129.92 | [12] |
| $Pt_3Cu_1$ aerogel | 38.77 | [13] |

Table S2. Chemical compositions of $PdO_x$ and Pd aerogels from EDS results (At. %)

| | **Pd** | **O** | **C** | **Pd/O** |
|---|---|---|---|---|
| **$PdO_x$ aerogels** | 7.08 | 11.86 | 81.06 | 0.60 |
| **Pd aerogels** | 23.69 | 5.88 | 70.43 | 4.03 |

Notably, the samples were modified on the ultrathin pure carbon film to perform the TEM characterization. Thus, a large amount of carbon could be detected in the corresponding EDS results.

Table S3. Ratios of metallic Pd and oxidized Pd species for Pd aerogels before and after *in situ* electrochemical activation

| | **Pd(0)** | **oxidized Pd** | **Pd(0)/ $PdO_x$** |
|---|---|---|---|
| **$PdO_x$ aerogels** | 0 | 1 | 0 |
| **Pd aerogels** | 0.655 | 0.345 | 1.9 |

Table S4. Comparison in electrocatalytic oxidation of methanol and ethanol with different Pd-based catalysts.

| Sample | MOR | EOR | Mass activity | Reference |
|---|---|---|---|---|
| Pd aerogel | 1 M KOH + 1 M methanol | | 2.99 A $mg^{-1}_{Pd}$ | This work |
| Pd aerogel | | 1 M KOH + 1M ethanol | 8.81 A $mg^{-1}_{Pd}$ | This work |
| $Pd_3Pb$ NSAs/C | 1 M KOH + 1 M methanol | | 2.98 A $mg^{-1}_{Pd}$ | [14] |
| $Pd_{0.52}Ag$/CNTs | 0.5 M NaOH + 1 M methanol | | 1.38 A $mg^{-1}_{Pd}$ | [15] |
| $Pd_4Sn$ WNWs/C | 0.1 M KOH + 0.5 M methanol | | 1.04 A $mg^{-1}_{Pd}$ | [16] |
| Pd NPs/Ni-Eth | 1 M NaOH + 0.5 M methanol | | 1.022 A $mg^{-1}_{Pd}$ | [17] |
| Pd-PdO PNTs-260 | 1 M KOH + 1 M methanol | | 1.111 A $mg^{-1}_{Pd}$ | [18] |
| Pd-$CeO_2$/NMCS | 1 M KOH + 1 M methanol | | 1.5 A $mg^{-1}_{Pd}$ | [19] |
| PdPtAu@Pd | 0.5 M KOH + 1 M methanol | | 2.266 A $mg^{-1}_{metal}$ | [20] |
| $Pd_{40}Ni_{43}P_{17}$ | | 1 M NaOH + 1 M ethanol | 4.95 A $mg^{-1}_{Pd}$ | [21] |
| Pd/NCB@NGS-2 | | 1 M KOH + 1 M ethanol | 2.69 A $mg^{-1}_{Pd}$ | [22] |
| Ag@$Pd_2P_{0.2}$ | | 1 M KOH + 1 M ethanol | 7.24 A $mg^{-1}_{Pd}$ | [23] |
| c-Pd-Ni-P@a-Pd-Ni-P | | 1 M KOH + 1 M ethanol | 3.05 A $mg^{-1}_{Pd}$ | [24] |
| $^{CG}Cu_1Pd_1/^{SD}Ir_{0.03}$ NSs/NPG | | 1 M KOH + 1 M ethanol | 7.105 A $mg^{-1}_{Pd}$ | [25] |
| Pd-Au HNS/C | | 1 M KOH + 1 M ethanol | 8.0 A $mg^{-1}_{Pd+Au}$ | [26] |

| | | | |
|---|---|---|---|
| Pd NPs@Ni SAC | 1 M KOH + 1 M ethanol | 1.093 A $mg^{-1}_{Pd}$ | [27] |

Table S5. Comparison of onset potentials for $PdO_x$, Pd aerogels and Pd/C towards the oxidation of various fuels.

| Fuels | Onset potential / V (vs. Ag/AgCl) | | |
|---|---|---|---|
| | $PdO_x$ aerogels | Pd aerogels | Pd/C |
| methanol | -0.626 | -0.686 | -0.618 |
| ethanol | -0.689 | -0.716 | -0.663 |
| isopropanol | -0.677 | -0.683 | -0.673 |
| ethylene glycol | -0.641 | -0.706 | -0.626 |
| glycerol | -0.698 | -0.701 | -0.678 |
| formic acid | <−0.8 | <−0.8 | <−0.8 |
| glucose | -0.703 | -0.745 | −0.699 |

**Reference:**


[1] X. Fan, B. Cai, R. Du, R. Hübner, M. Georgi, G. Jiang, L. Li, M. Samadi Khoshkhoo, H. Sun, A. Eychmüller, Chem. Mater. 2019, 31, 10094-10099.

[2] D. Wen, A.-K. Herrmann, L. Borchardt, F. Simon, W. Liu, S. Kaskel, A. Eychmüller, J. Am. Chem. Soc. 2014, 136, 2727-2730.

[3] R. Du, J. O. Joswig, X. Fan, R. Hubner, D. Spittel, Y. Hu, A. Eychmuller, Matter 2020, 2, 908–920.

[4] R. Du, J.-O. Joswig, R. Hübner, L. Zhou, W. Wei, Y. Hu, A. Eychmüller, Angew. Chem. Int. Ed. 2020, 59, 8293-8300.

[5] S. Naskar, A. Freytag, J. Deutsch, N. Wendt, P. Behrens, A. Kockritz, N. C. Bigall, Chem. Mater. 2017, 29, 9208-9217.

[6] R. Du, Y. Hu, R. Hübner, J. O. Joswig, X. Fan, K. Schneider, A. Eychmüller, Sci. Adv. 2019, 5, eaaw4590.

[7] R. Du, J. Wang, Y. Wang, R. Hübner, X. Fan, I. Senkovska, Y. Hu, S. Kaskel, A. Eychmüller, Nat. Commun. 2020, 11, 1590.

[8] H. J. Wang, S. L. Zhang, W. W. Cai, B. Z. Xu, Z. X. Cai, Y. Wu, X. Luo, X. Q. Wei, Z. Liu, W. L. Gu, A. Eychmuller, C. Z. Zhu, J. Chen, Mater. Horizons 2020, 7, 2407-2413.

[9] X. L. Fan, S. Zerebecki, R. Du, R. Hubner, G. Marzum, G. C. Jiang, Y. Hu, S.

Barcikowki, S. Reichenberger, A. Eychmuller, Angew. Chem. Int. Ed. 2020, 59, 5706-5711.

[10] B. Cai, A. Dianat, R. Hubner, W. Liu, D. Wen, A. Benad, L. Sonntag, T. Gemming, G. Cuniberti, A. Eychmuller, Adv. Mater. 2017, 29, 1605254.

[11] R. Zhang, L. Zhu, X. Liu, J. Zhu, Y. Zhao, ACS Sustain. Chem. Eng. 2021, 9, 7837–7845.

[12] Z. Lin, S. Liu, Y. Liu, Z. Liu, S. Zhang, X. Zhang, Y. Tian, Z. Tang, J. Power Sources 2021, 514, 230600.

[13] X. G. Tie, X. H. Sun, Q. X. Li, Y. L. Min, Q. J. Xu, J. Electrochem. Soc. 2022, 169, 026517.

[14] L. Z. Bu, C. Y. Tang, Q. Shao, X. Zhu, X. Q. Huang, ACS Catal. 2018, 8, 4569-4575.

[15] L. Huang, J. S. Zou, J. Y. Ye, Z. Y. Zhou, Z. Lin, X. W. Kang, P. K. Jain, S. W. Chen, Angew. Chem. Int. Ed. 2019, 58, 8794-8798.

[16] Y. Zhang, B. L. Huang, Q. Shao, Y. G. Feng, L. K. Xiong, Y. Peng, X. Q. Huang, Nano Lett. 2019, 19, 6894-6903.

[17] H. Lei, X. T. Li, C. B. Sun, J. R. Zeng, S. S. Siwal, Q. B. Zhang, Small 2019, 15, 1804722.

[18] T. J. Wang, F. M. Li, H. Huang, S. W. Yin, P. Chen, P. J. Jin, Y. Chen, Adv. Funct. Mater. 2020, 30, 2000534.

[19] Q. Tan, C. Y. Shu, J. Abbott, Q. F. Zhao, L. T. Liu, T. Qu, Y. Z. Chen, H. Y. Zhu, Y. N. Liu, G. Wu, ACS Catal. 2019, 9, 6362-6371.

[20] F. Gao, Y. Zhang, H. You, Z. Li, B. Zou, Y. Du, Chem. Commun. 2021, 57, 13198-13201.

[21] L. Chen, L. L. Lu, H. L. Zhu, Y. G. Chen, Y. Huang, Y. D. Li, L. Y. Wang, Nat. Commun. 2017, 8, 14136.

[22] S. W. Li, J. H. Shu, S. Z. Ma, H. L. Yang, J. Jin, X. H. Zhang, R. F. Jin, Appl. Catal. B-Environ. 2021, 280, 119464.

[23] X. B. Yang, Z. P. Liang, S. Chen, M. J. Ma, Q. Wang, X. L. Tong, Q. H. Zhang, J. Y. Ye, L. Gu, N. J. Yang, Small 2020, 16, 2004727.

[24] P. F. Yin, M. Zhou, J. Z. Chen, C. L. Tan, G. G. Liu, Q. L. Ma, Q. B. Yun, X.

Zhang, H. F. Cheng, Q. P. Lu, B. Chen, Y. Chen, Z. C. Zhang, J. T. Huang, D. Y. Hu, J. Wang, Q. Liu, Z. Y. Luo, Z. Q. Liu, Y. Y. Ge, X. J. Wu, X. W. Du, H. Zhang, Adv. Mater. 2020, 32, 2000482.

[25] L. X. Luo, C. H. Fu, F. Yang, X. L. Li, F. L. Jiang, Y. G. Guo, F. J. Zhu, L. J. Yang, S. Y. Shen, J. L. Zhang, ACS Catal. 2020, 10, 1171-1184.

[26] F. Lv, W. Y. Zhang, M. Z. Sun, F. X. Lin, T. Wu, P. Zhou, W. X. Yang, P. Gao, B. L. Huang, S. J. Guo, Adv. Energy Mater. 2021, 11, 2100187.

[27] S. Li, A. Guan, H. Wang, Y. Yan, H. Huang, C. Jing, L. Zhang, L. Zhang, G. Zheng, J. Mater. Chem. A 2022, 10, 6129-6133.